

Variation of the X-ray non-thermal emission in the Arches cloud

M. Clavel,^{1,2*} S. Soldi,¹ R. Terrier,¹ V. Tatischeff,³ G. Maurin,⁴ G. Ponti,⁵
A. Goldwurm^{1,2} and A. Decourchelle^{6,2}

¹ *AstroParticule et Cosmologie, Université Paris Diderot, CNRS/IN2P3, CEA/DSM, Observatoire de Paris, Sorbonne Paris Cité; 10, rue Alice Domon et Léonie Duquet, 75205 Paris Cedex 13, France*

² *Service d'Astrophysique/IRFU/DSM, CEA Saclay; Bât. 709, 91191 Gif-sur-Yvette Cedex, France*

³ *Centre de Sciences Nucléaires et de Sciences de la Matière, CNRS/IN2P3, Université Paris-Sud; 91405 Orsay, France*

⁴ *Laboratoire d'Annecy-le-Vieux de Physique des Particules, Université de Savoie, CNRS/IN2P3; 74941 Annecy-le-Vieux, France*

⁵ *Max-Planck-Institute for Extraterrestrial Physics, Garching, PSF 1312, 85741 Garching, Germany*

⁶ *Laboratoire AIM (CEA/Irfu, CNRS/INSU, Université Paris VII), CEA Saclay; Bât. 709, 91191 Gif-sur-Yvette Cedex, France*

Accepted 2014 June 19. Received 2014 June 19; in original form 2014 May 30

ABSTRACT

The origin of the iron fluorescent line at 6.4 keV from an extended region surrounding the Arches cluster is debated and the non-variability of this emission up to 2009 has favored the low-energy cosmic-ray origin over a possible irradiation by hard X-rays. By probing the variability of the Arches cloud non-thermal emission in the most recent years, including a deep observation in 2012, we intend to discriminate between the two competing scenarios. We perform a spectral fit of *XMM-Newton* observations collected from 2000 to 2013 in order to build the Arches cloud lightcurve corresponding to both the neutral Fe K α line and the X-ray continuum emissions. We reveal a 30% flux drop in 2012, detected with more than 4σ significance for both components. This implies that a large fraction of the studied non-thermal emission is due to the reflection of an X-ray transient source.

Key words: Galaxy: center – X-ray: ISM – ISM: clouds – Cosmic rays

1 INTRODUCTION

The Arches cluster is a massive star cluster located within the Galactic center region, at about 11' to the Galactic north-east of Sagittarius A*. The X-ray emission of the cluster is associated with a thermal component that is thought to originate from collisions of winds from massive stars (Yusef-Zadeh et al. 2002; Wang, Dong, & Lang 2006; Tsujimoto, Hyodo, & Koyama 2007). A diffuse and more extended non thermal emission including the neutral iron fluorescent line at 6.4 keV, has also been detected from a region directly surrounding the star cluster. This emission could be created either by the interaction of low-energy hadronic cosmic-rays with molecular material surrounding the cluster (Tatischeff, Decourchelle, & Maurin 2012) or by a strong X-ray irradiation as in other clouds of the central molecular zone (CMZ; Clavel et al. 2013; Ponti et al. 2013, and references therein). Both scenarios are compatible with the *XMM-Newton* observations collected up to 2009 (Capelli et al. 2011b; Tatischeff, Decourchelle, & Maurin 2012) and also with the latest *NuSTAR* characterization

of the higher-energy emission (Krivonos et al. 2014). However, due to the constant Fe K α line emission and the absence of clear molecular counterpart of the X-ray emission, the low-energy cosmic-ray protons scenario has been favored (Tatischeff, Decourchelle, & Maurin 2012).

In this paper, we add *XMM-Newton* observations spanning three years more compared to the previous studies of the Arches non-thermal emission. In particular, we include data from the 2013 monitoring of Sgr A* and a deep observation obtained in 2012 during a scan of the CMZ. We find a significant decrease of both the 6.4 keV and the continuum emissions in the 2012 data set, suggesting that a significant part of the non-thermal emission is due to reflection. In Section 2, we present the data and its reduction. The results of our analysis are detailed in Section 3, and the origin of the non-thermal emission is discussed in Section 4.

2 XMM-NEWTON OBSERVATIONS AND DATA REDUCTION

We analyzed all the *XMM-Newton*/EPIC observations available since 2000 and including the Arches cluster region (re-

* E-mail: maica.clavel@apc.univ-paris7.fr (MC)

ported in Tab. A1). The data reduction was carried out using the *XMM-Newton* Extended Source Analysis Software (ESAS, Snowden et al. 2008) included in version 12.0.1 of the *XMM-Newton* Science Analysis Software (SAS). Calibrated event lists were produced for each exposure using the SAS *emchain* and *epchain* scripts and ESAS *mos-filter* and *pn-filter* were used to exclude periods affected by soft proton flaring.

Background- and continuum-subtracted mosaic images have been created in the energy band 6.32–6.48 keV (Fig. 1). To produce them, we created the quiescent particle background (QPB) images, the count images and model exposure maps for each observation and each instrument, using *mos-spectra*, *pn-spectra*, *mos-back* and *pn-back* in the two energy bands 6.32–6.48 keV and 3–6 keV. The combined exposure map was computed taking into account the different efficiencies of the three instruments. The contribution of the continuum to the 6.4 keV line was estimated using the extrapolation of the 3–6 keV emission and assuming an absorbed power-law spectrum with a photon index $\Gamma = 2$ and a column density $N_H = 7 \times 10^{22} \text{ cm}^{-2}$. The *Chandra* analysis tool *reproject_image_grid* was used to correctly reproject the maps of each instrument and each observation within the same year and to mosaic them. For each year, the total background mosaic and the estimated continuum mosaic were then subtracted from the 6.4 keV count mosaic and normalized by the total exposure to obtain the final count rate mosaics.

All spectra used in the analysis were extracted with the ESAS *mos-spectra* and *pn-spectra* scripts. In particular, the region defined to study the variability of the X-ray emission corresponds to the elliptical region where the brightest 6.4 keV emission is detected (largest ellipse in Fig. 1, referred as ‘Cloud’ in Tab. 1). The Arches cluster (blue ellipse in Fig. 1, referred as ‘Cluster’ in Tab. 1) has been excluded from the former region for the analysis. We point out that this spectral extraction region is very similar to the one used in Tatischeff, Decourchelle, & Maurin (2012). The QPB was obtained using filter wheel closed event lists provided by the ESAS calibration database. For each region, background spectra were extracted for each EPIC camera at the same position in instrumental coordinates using the *pn-spectra* and *mos-spectra* tasks. These spectra were then normalized to the level of QPB in the observations, using *pn-back* and *mos-back*. Spectrum counts are grouped to have at least thirty counts per bin and then fitted using modified chi-square statistics. The errors are given by the confidence interval of the fits at 1σ .

In order to study the astrophysical background contributing to the measured flux we extracted spectra from several large regions surrounding the Arches cloud and fitted the corresponding spectra with a two-thermal-plasma model accounting for the Galactic thermal emission (at 1 and 7 keV, Munro et al. 2004). The ratio between the normalization of the soft and of the hot components has different values depending on the region we consider. This difference is to be linked to the strong anisotropy of the spatial distribution of the soft emission. Therefore, getting a precise estimate of the astrophysical background at the position of the Arches cloud is not straightforward. Nevertheless, using an elliptical region (referenced as ‘Bkg test’ in Tab. 1) that has a sufficient coverage for all years, we fit-

Table 1. Elliptical regions used for the spectral extraction.

Region	l [°]	b [°]	Axes [″]	Angle [°]
Cloud	0.124	0.018	58.9, 25.1	125.4
Cluster (excl.)	0.123	0.019	16.0, 14.0	58.6
Bkg test	0.134	−0.031	100.8, 48.3	125.42
NuStar	0.122	0.019	50, 50	–

ted the normalization of the hot plasma (fixing the ratio between the two components at its mean value of 5.5). The weighted average of the hot plasma normalization is then $I_{7\text{keV}} = 11.4 \pm 0.3 \times 10^{-4} \text{ cm}^{-5}$ with a maximal amplitude for the variation lower than 6.6%.

To account for the emission of the Arches cloud region we used the following model,

$$\text{WABS} \times (\text{APEC} + \text{POWERLAW}) + \text{GAUSSIAN}. \quad (1)$$

A similar model was used by Tatischeff, Decourchelle, & Maurin (2012) but here we do not correct the iron line emission for the overall absorption¹. According to the parameters derived for the Arches cloud from the overall *XMM-Newton* data set (Table 3 in Tatischeff, Decourchelle, & Maurin 2012), we fixed the temperature of the plasma component (APEC) to $kT = 2.2 \text{ keV}$, the cloud metallicity to $Z = 1.7 Z_\odot$, the index of the POWERLAW to $\Gamma = 1.6$, the centroid energy and width of the GAUSSIAN to $E_{6.4\text{keV}} = 6.4 \text{ keV}$ and $\Delta E_{6.4\text{keV}} = 10 \text{ eV}$, respectively. The free parameters are therefore the overall absorption and the normalizations of the plasma, of the line and of the reflection continuum components. For each year, we fit these four parameters between 2 and 7.5 keV on all spectra simultaneously. All fits were satisfactory, giving reduced $\chi^2 \sim 1$. We also tested a similar model including two thermal plasma at 1 and 7 keV, respectively, in order to better account for the astrophysical background present in the data. This second model gave consistent results regarding the Fe $K\alpha$ line emission. Interpreting the continuum component is more complex since it highly depends on the astrophysical background estimation. However, as discussed above, the steadiness of the astrophysical background is such that any variation larger than 10% can only be attributed to a variation of the Arches cloud emission.

3 VARIATION OF THE X-RAY NON-THERMAL EMISSION

Fig. 1 presents the Fe $K\alpha$ line emission of the Arches region for seven different years between 2000 and 2013 along with the best correlation found for the molecular material in the region. The overall X-ray emission is distributed within an elongated ellipse, centered on the Galactic east of the Arches cluster. This shape is fully consistent with the morphology of the N_2H^+ ($J=1-0$) emission seen by Mopra around -25 km s^{-1} (Jones et al. 2012). However, its exact

¹ The absorption correction relies on the N_H value fitted to the softer part of the spectrum, which also depends on the background subtraction. This would force the correlation between the line and the continuum emissions.

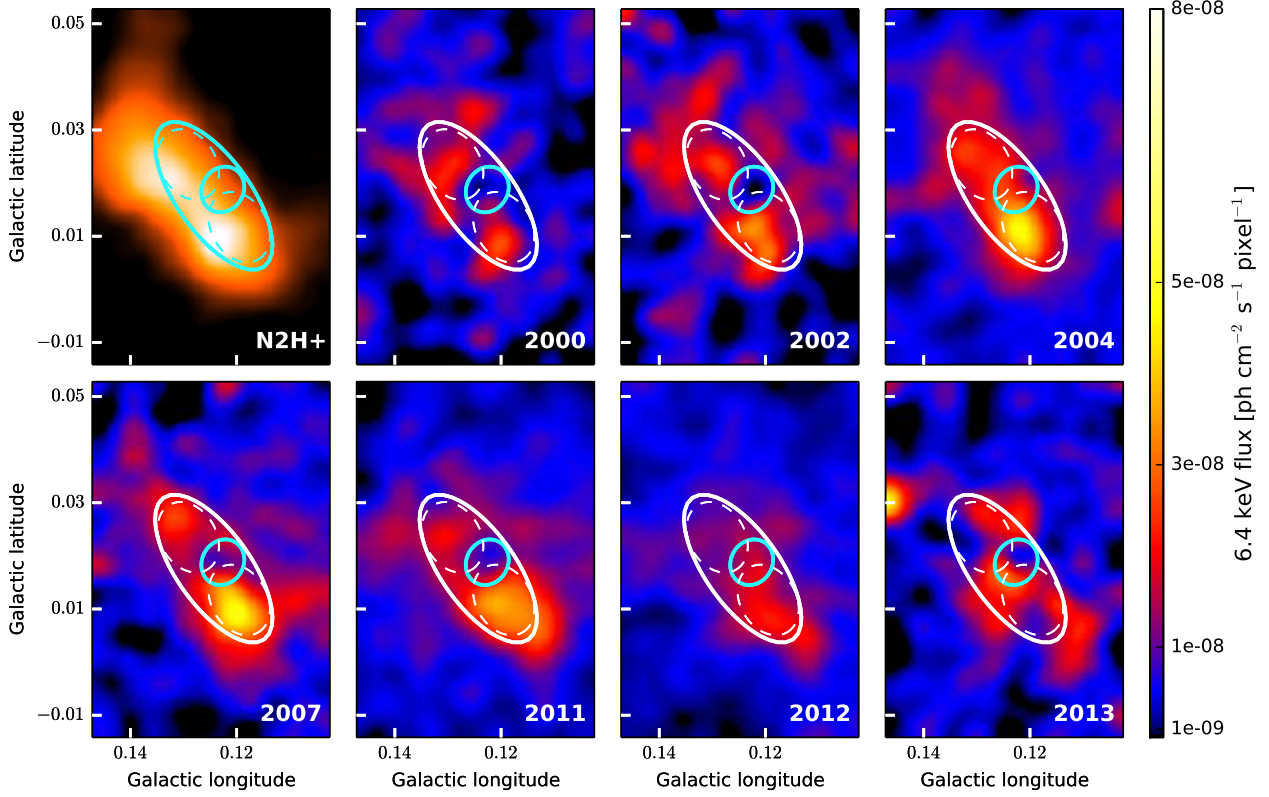


Figure 1. (*Top Left*) Mopra N_2H^+ map of the Arches cloud position integrated between -40 and -10 km s^{-1} (Jones et al. 2012). A significant molecular contribution is there albeit a slight shift of the molecular emission to the south east compared to the X-ray emission of the Arches region. (*Others*) Continuum and background subtracted Fe $\text{K}\alpha$ maps of the Arches cluster region for seven different years, from top left to bottom right: 2000, 2002, 2004, 2007, 2011, 2012 and 2013. The maps are displayed in Galactic coordinates and smoothed using a gaussian kernel of $20''$ radius. The solid white ellipse is the cloud region, the cyan ellipse is the cluster region, and the two dashed ellipses are two cloud subregions: north and south. The overall cloud shows morphological variations from period to period with a clear decrease in the overall emission in 2012.

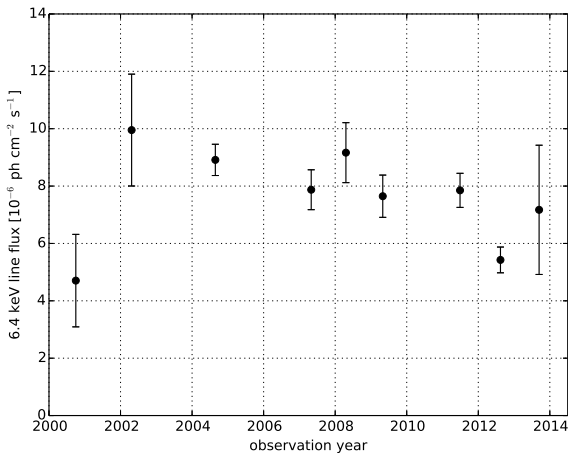


Figure 2. Fe $\text{K}\alpha$ line flux lightcurve of the Arches cloud. The emission is compatible with a constant emission up to 2011 with an average value of $F_{6.4\text{keV}} = 8.2 \times 10^{-6} \text{ ph cm}^{-2} \text{ s}^{-1}$ but the constant fit on the whole period is rejected at 4.3σ due to a more than 30% drop in 2012.

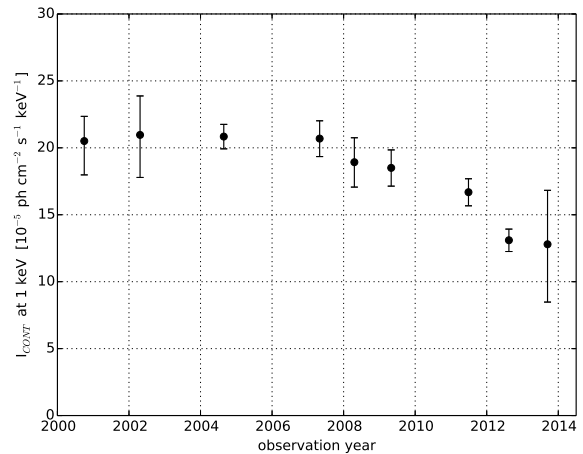


Figure 3. Continuum flux lightcurve associated with the power-law component of the Arches cloud. The lightcurve is compatible with a constant emission up to 2011 with an average value of $I_{\text{cont}} = 19.3 \times 10^{-5} \text{ ph cm}^{-2} \text{ s}^{-1} \text{ keV}^{-1}$ but the constant fit on the whole period is rejected at 5.6σ .

position is shifted by about $18''$ compared to the molecular data. This is larger than the $10''$ pointing error mentioned by Jones et al. (2012). Nevertheless, the higher antenna temperature in the Galactic south of the Arches ellipse is consistent with the brightest emission observed in the Fe K α line. This is in agreement with the fluxes reported by Capelli et al. (2011b), and with the position shift of the hard X-ray emission detected by Krivonos et al. (2014) using *NuSTAR*. We also point out that this south molecular core is not seen in the CS line at the corresponding velocity (Tsuboi, Handa, & Ukita 1999). This is a hint that the CS emission might be self absorbed at this position, indicating a rather dense core.

From Fig. 1 it is also clear that the Fe K α line emission is varying over the 2000–2013 time period with both morphological and intensity changes. In particular, both the north and south subregions of the Arches cloud (dashed ellipses) seem to be increasing and then decreasing in flux, with a peak in 2004 and 2007, respectively. In 2012, there is an overall decrease of the emission. In spite of a relatively shallow exposure in 2013, the overall morphology looks quite different from what is seen in the previous years, since the emission seems to surround the N₂H⁺ dense cores.

In order to confirm the variations seen in the images we performed spectral fits of the Arches cloud data (excluding the cluster) using the model detailed in Sec. 2. Figs. 2 and 3 present the variations of the Fe K α line flux and of the power-law continuum emission, respectively. Both components are varying significantly with a rejection of the constant fit at 4.3 and 5.6σ , respectively, and both have dropped by more than 30% in 2012. When a Pearson correlation test is applied to the power-law continuum flux as a function of the 6.4 keV flux (following the prescription of Pozzi, Di Matteo, & Aste 2012 to take uncertainties into account), a correlation is detected at 3σ confidence level and the linear fit results in a slope of 1.0 ± 0.3 , indicating that most of the power-law continuum is indeed linked to the 6.4 keV emission. As expected in this case, the equivalent width of the Fe K α line is compatible with being constant over time with an average value $EW = 0.9 \pm 0.1$ keV (rejection at less than 0.2σ). The two other free parameters of the spectral fit are compatible with being constant over the thirteen-year period and the weighted mean values are $N_H = 6.0 \pm 0.3 \times 10^{22} \text{ cm}^{-2}$ for the absorption and $I_{2.2\text{keV}} = 3.6 \pm 0.7 \times 10^{-4} \text{ cm}^{-5}$ for the normalization of the thermal plasma. We point out that the normalization of the plasma given here does not consider the 2007 value that is significantly higher due to a contamination from the flaring cluster (Capelli et al. 2011a).

To compare our values to the ones presented in Tatischeff, Decourchelle, & Maurin (2012), we also divided the 2004 data set in two time periods and performed a constant fit of the data up to 2009. For this restricted data set, both the Fe K α line flux and the power-law continuum normalization are compatible with being constant (rejection at less than 1.4σ) and result in $F_{6.4\text{keV}} = 8.3 \pm 1.0 \times 10^{-6} \text{ ph cm}^{-2} \text{ s}^{-1}$ (9.6 ± 1.0 , if corrected for the absorption) and $I_{\text{cont}} = 20.1 \pm 1.6 \times 10^{-5} \text{ ph cm}^{-2} \text{ s}^{-1} \text{ keV}^{-1}$, respectively. Both values are compatible with Tatischeff, Decourchelle, & Maurin (2012) results even if the continuum component cannot be directly compared due to different background estimations in the

two analyses. The individual data points are also compatible within the error bars, except for the 2000 point for which values are about 2σ apart. We can exclude that this discrepancy is due to a different position of the source within the field of view compared to the 2002–2009 observations. Indeed the systematic error associated² is negligible compared to the 1σ error bars given by the fit. The difference is most likely due to the poor quality of the corresponding data set but it has not been fully identified. In any case, we point out that excluding the 2000 data point does not change the significance of the constant fit rejection.

The *XMM-Newton* observations of autumn 2012 can also be compared to the *NuSTAR* observations collected in the same period (Krivonos et al. 2014). To do so, we extracted spectra from a circular region of $50''$ radius centered on the cluster (referred as ‘NuStar’ in Tab. 1) and fitted them with the same model (eq. 1) but fixing the overall absorption, the temperature of the plasma and the index of the power-law to the *NuSTAR* values (Table 5 and Model 1 in Krivonos et al. 2014). The values found for the Fe K α line flux (corrected for absorption, $F_{6.4\text{keV}} = 1.02 \pm 0.06 \times 10^{-5} \text{ ph cm}^{-2} \text{ s}^{-1}$), for the normalization of the plasma ($I_{1.76\text{keV}} = 50 \pm 1 \times 10^{-4} \text{ cm}^{-5}$) and of the continuum ($I_{\text{cont}} = 1.58 \pm 0.08 \times 10^{-12} \text{ erg cm}^{-2} \text{ s}^{-1}$ over 3–20 keV) are fully compatible with the values stated by Krivonos et al. (2014) for the same region. Since the absolute cross calibration factor between *XMM-Newton* and *NuSTAR* is less than 3% (Risaliti et al. 2013), we infer that the apparent consistency between Tatischeff, Decourchelle, & Maurin (2012) and Krivonos et al. (2014) fluxes is to be linked to the larger region considered in the later work. The *NuSTAR* value is therefore consistent with the 2012 emission drop.

4 DISCUSSION: ORIGIN OF THE NON-THERMAL EMISSION

The non-thermal emission measured in the region surrounding the Arches cluster could be created by either a particle bombardment or a strong hard X-ray irradiation by an external source. Since the spectrum of the Arches cloud does not provide enough information to discriminate between the two models (Capelli et al. 2011b; Tatischeff, Decourchelle, & Maurin 2012; Krivonos et al. 2014), the remaining diagnostics are linked to the location of the emission and its variability.

The absence of correlation between this non-thermal X-ray emission and known molecular features at other wavelengths was supporting the particle bombardment scenario. In this work we identified for the first time a relevant molecular counterpart of the 6.4 keV emission using the N₂H⁺ tracer. In particular, the overall morphology of the molecular structure with a two-lobe shape is in good agreement with the X-ray image. This supports the reflection scenario. The peak to peak correlation is not fully verified because of the slight shift mentioned in Section 3. However, the exact

² This systematic error is related to the effective area of the EPIC camera (Tatischeff, Decourchelle, & Maurin 2012). We tested this effect on our data set by computing the flux of the Sgr A East region as a function of its offset within the detector. We found a maximal amplitude $< 4\%$ for this systematic.

distribution of the gas might be different than the one given by this molecular tracer, and the complex propagation of the X-ray signal within this structure may also account for the displacement (Clavel et al. 2013).

Furthermore, the 30% decrease within about one year, detected for both the 6.4 keV line and the continuum emissions, can only be explained by the reflection of hard X-ray irradiation. Indeed, the diffusion timescale and the possible rate of energy losses of the low-energy cosmic ray protons only allow for an emission decrease on much longer time scales (decades) and the energetic required for low-energy cosmic ray electrons is not realistic (Tatischeff, Decourchelle, & Maurin 2012). Therefore, the significant variation of the non-thermal emission detected for the first time in the present work is the key element to conclude that a significant fraction of this emission is due to reflection.

The source at the origin of the X-ray emission from the Arches cloud is unlikely to be located within the Arches cluster (Capelli et al. 2011b; Tatischeff, Decourchelle, & Maurin 2012). Moreover, the variability observed is not isolated since variations have already been observed in nearby structures (Capelli et al. 2011b) and, on larger scale, within the Sgr A region (Ponti et al. 2010; Clavel et al. 2013). A large fraction of the non-thermal emission of the Arches cloud is therefore likely due to the past activity of Sgr A*, as is the emission of most of the regions listed above.

ACKNOWLEDGMENTS

The scientific results reported in this article are based on observations obtained with *XMM-Newton*, an ESA science mission with instruments and contributions directly funded by ESA Member States and NASA. The molecular map was obtained using the Mopra radio telescope, a part of the Australia Telescope National Facility which is funded by the Commonwealth of Australia for operation as a National Facility managed by CSIRO. M.C. acknowledges the Université Paris Sud 11 for financial support. S.S. acknowledges the Centre National d'Etudes Spatiales (CNES) for financial support. G.P. acknowledges support via an EU Marie Curie Intra-European fellowship under contract no. FP-PEOPLE-2012-IEF-331095. Partial support through the COST action MP0905 Black Holes in a Violent Universe is acknowledged.

REFERENCES

- Capelli R., Warwick R. S., Cappelluti N., Gillessen S., Predehl P., Porquet D., Czesla S., 2011a, *A&A*, 525, L2
 Capelli R., Warwick R. S., Porquet D., Gillessen S., Predehl P., 2011b, *A&A*, 530, A38
 Clavel M., Terrier R., Goldwurm A., Morris M. R., Ponti G., Soldi S., Trap G., 2013, *A&A*, 558, A32
 Jones P. A., et al., 2012, *MNRAS*, 419, 2961
 Krivonos R. A., et al., 2014, *ApJ*, 781, 107
 Munro M. P., et al., 2004, *ApJ*, 613, 326
 Ponti G., Terrier R., Goldwurm A., Belanger G., Trap G., 2010, *ApJ*, 714, 732

Table A1. *XMM-Newton* observations used in the present work.

Date	Obs. ID	Exposure ^a [ks]			Coverage ^b		
		m1	m2	pn	m1	m2	pn
2000-09-19	0112970401	22.2	22.1	18.6	1.00	1.00	0.90
2000-09-21	0112970501	14.0	14.6	5.3	0.97	0.99	0.91
2002-02-26	0111350101	42.2	41.5	38.5	1.00	1.00	0.64
2002-10-03	0111350301	7.5	7.9	6.4	0.99	1.00	0.53
2004-03-28	0202670501	32.9	30.4	14.8	1.00	1.00	1.00
2004-03-30	0202670601	32.6	35.2	25.6	1.00	1.00	0.99
2004-08-31	0202670701	78.8	84.5	59.5	1.00	0.99	1.00
2004-09-02	0202670801	94.6	98.6	70.0	1.00	0.98	1.00
2007-02-27	0506291201	22.7	24.8	0	1.00	0.90	0
2007-03-30	0402430701	26.3	28.0	18.1	0	1.00	1.00
2007-04-01	0402430301	60.7	62.9	53.3	0	1.00	0.99
2007-04-03	0402430401	40.6	41.2	26.7	0	1.00	1.00
2007-09-06	0504940201	8.9	9.3	5.9	1.00	1.00	0.39
2008-03-23	0505670101	73.5	74.3	49.0	0	1.00	1.00
2009-04-01	0554750401	32.4	33.5	30.2	0	1.00	1.00
2009-04-03	0554750501	41.0	41.6	36.6	0	1.00	0.99
2009-04-05	0554750601	37.0	36.8	28.7	0	1.00	0.99
2011-03-28	0604300601	31.3	32.7	24.1	0	1.00	0.99
2011-03-30	0604300701	37.3	41.9	22.6	0	1.00	1.00
2011-04-01	0604300801	35.1	34.9	31.5	0	1.00	1.00
2011-04-03	0604300901	21.4	22.4	15.3	0	1.00	0.99
2011-04-05	0604301001	39.8	41.6	23.6	0	1.00	0.99
2011-08-31	0658600101	47.6	48.0	45.2	1.00	1.00	0.45
2011-09-01	0658600201	40.4	43.0	37.0	1.00	1.00	0.47
2012-03-13	0674600601	9.1	10.2	8.1	0	1.00	0.90
2012-03-15	0674600701	13.5	14.4	8.9	0	1.00	0.93
2012-03-17	0674601101	10.7	11.1	7.0	0	1.00	0.98
2012-03-19	0674600801	18.3	18.5	15.2	0	1.00	0.99
2012-03-21	0674601001	20.9	21.6	17.4	0	1.00	1.00
2012-08-31	0694640301	40.1	40.1	38.6	0	0.36	0.57
2012-09-02	0694640401	44.4	44.0	13.1	0.97	1.00	0.88
2012-09-24	0694641101	39.7	39.8	38.8	0.95	0.94	0.88
2012-09-26	0694641201	39.8	40.5	38.2	1.00	0.90	1.00
2013-08-30	0724210201	42.6	43.7	40.5	0	1.00	0.50
2013-09-22	0724210501	32.7	32.9	26.5	0	1.00	0.48

^a Clean exposure at the Arches cloud position, for each of the EPIC camera instruments: MOS1 (m1), MOS2 (m2) and PN (pn).

^b Fraction of the Arches cloud region covered by the observations.

- Ponti G., Morris M. R., Terrier R., Goldwurm A., 2013, *ASSP*, 34, 331
 Pozzi F., Di Matteo T., Aste T., 2012, *EPJB*, 85, 175
 Risaliti G., et al., 2013, *Nature*, 494, 449
 Snowden S. L., Mushotzky R. F., Kuntz K. D., Davis D. S., 2008, *A&A*, 478, 615
 Tatischeff V., Decourchelle A., Maurin G., 2012, *A&A*, 546, A88
 Tsuboi M., Handa T., Ukita N., 1999, *ApJS*, 120, 1
 Tsujimoto M., Hyodo Y., Koyama K., 2007, *PASJ*, 59, 229
 Wang Q. D., Dong H., Lang C., 2006, *MNRAS*, 371, 38
 Yusef-Zadeh F., Law C., Wardle M., Wang Q. D., Fruscione A., Lang C. C., Cotera A., 2002, *ApJ*, 570, 665

APPENDIX A: OBSERVATION SELECTION

The observations used in the analysis are listed in Tab. A1, along with the corresponding clean exposure and the fraction of the Arches cloud region covered by each instrument. Any instrument presenting either less than 7 ks clean exposure or less than 80% coverage has been discarded from the spectral analysis. We preferred to exclude observations with a low coverage in order to avoid a bias due to the non uniform spatial distribution of the emission within the region.